Journal of Quantitative Spectroscopy & Radiative Transfer 278 (2022) 108020

Contents lists available at ScienceDirect

Journal of Quantitative Spectroscopy & Radiative Transfer

journal homepage: www.elsevier.com/locate/jqsrt

Compton double ionization of the helium atom: Can it be a method of dynamical spectroscopy of ground state electron correlation?

O. Chuluunbaatar[a,b], S. Houamer[c,*], Yu.V. Popov[d,a], I.P. Volobuev[d], M. Kircher[e], R. Dörner[e]

[a] Joint Institute of Nuclear Research, Dubna, Moscow Region 141980, Russia
[b] Institute of Mathematics and Digital Technology, Mongolian Academy of Sciences, Ulaanbaatar 13330, Mongolia
[c] LPQSD, Faculty of Science, University Setif-1, Setif, 19000, Algeria
[d] Skobeltsyn Institute of Nuclear Physics, Lomonosov Moscow State University, Moscow 119991, Russia
[e] Institut für Kernphysik, J. W. Goethe Universität, Max-von-Laue-Str. 1, D-60438 Frankfurt, Germany

ARTICLE INFO

Article history:
Received 21 October 2021
Revised 26 November 2021
Accepted 26 November 2021
Available online 27 November 2021

Keywords:
Methods of dynamical spectroscopy
Compton double ionization of atoms

ABSTRACT

Recent experiments on single and double ionization of atoms by Compton scattering potentially open the door to establishing new methods of dynamical spectroscopy complementing the well-known methods like (e,2e) and (e,3e) spectroscopy. In this paper we explore the possibility to use double ionization of the helium atom by Compton scattering as a tool for direct spectroscopy of electron-electron correlations. For rather high photon energies of a few dozens of keV, a non-relativistic theoretical description of the process and the Kramers-Heisenberg-Waller approximation can be consistently used with a high computational efficiency.

1. Introduction

In the present paper we study the double ionization of the helium atom by Compton scattering of a photon with energies of several tens of keV. At these incident photon energies the scattering by helium atoms can be described in the non-relativistic approximation. This paper is a direct continuation of our previous paper, where the Compton single ionization was substantiated as a method of momentum spectroscopy of the active electron in an atomic target [1].

From the beginning of atomic physics the atomic structure was usually studied by high-resolution spectroscopy. Alternatively to measuring energies of bound and excited states, one can also study fragmentation processes and obtain a detailed structure information from the fragment momentum distributions. To this end the photoelectric effect (see [2] for a recent example), or charged particle impact is mostly used nowadays. In these studies, a well established technique is $(e, 2e)$ coincidence spectroscopy at large momentum transfer (the so called Electron Momentum Spectroscopy – EMS) which allows to investigate the momentum distribution of the active electron in the target [3,4], whereas $(e, 3e)$ and $(e, 3-1e)$ reactions at large momentum transfer give valuable information about the electron pair correlations [5,6]. For the latter reactions their fully differential cross sections (and even the partial integral ones) are much smaller than the differential cross sections for single ionization reactions. The measurement of these small cross sections is experimentally very challenging, in particular, these experiments require coincidence detection of the particles in the final state of the reactions.

In the case under consideration, an energetic photon is used instead of a fast incident electron, which, in Compton scattering, is treated as a relativistic particle with a special dispersion relation. The coincidence method based on simultaneous detection of the ejected electron and the scattered photon was first used by Bothe and Geiger [7] in 1924, i.e., just two years after the experiments of A. Compton. The aim of Bothe's experiment was to verify, whether the ejected electrons which were earlier detected, (for example, with the help of the Wilson chamber) were really emitted from the target simultaneously with the scattering of photons. He also intended to test, whether energy and momentum conservation law in the microcosm holds for each single event rather than only for mean values as speculated by Bohr, Kramers and Slater [8]. The idea of the coincidence method is to register the particles in the final state with a given space or time correlation between them. To detect the particles flying in certain directions, several counters are installed in their way, which are connected to a coincidence circuit device selecting those events, where the signal comes from all the counters within a certain short time interval.

* Corresponding author.
E-mail address: s_houamer@univ-setif.dz (S. Houamer).

https://doi.org/10.1016/j.jqsrt.2021.108020
0022-4073/

For example, in Bothe's experiment discharge counters were connected to quartz fiber electrometers. The deflection of the fibers was recorded by a moving film, and, as a result, Bothe could distinguish the discharges with 1 ms time resolution. In 1954 Bothe was awarded the Nobel Prize "for the coincidence method and his discoveries made therewith".

Despite the low efficiency of such measurements, the coincidence method, with certain technical improvements, was used for studying the electron states of target atoms for almost 100 years. However, it is currently impossible to use the electron-photon coincidence method, which was implemented in Bothe's experiment, for precision measurements with gas phase target. For example, a small value of the total cross section of single ionization reactions (of the order of 1 barn) and small solid angles of particle collection typical for most photon detectors did not give the possibility to carry out experiments on Compton scattering from free atoms and molecules up to the present time.

An alternative to detecting the momentum of the scattered photon and the electron is offered by the COLTRIMS (COLd Target Recoil Ion Momentum Spectroscopy) [9] technique. It allows one to simultaneously measure the momenta of the emitted electron and recoil ion, which both can be collected with the total solid angle $\Omega_{total} = 4\pi$. The momentum of the scattered photon can be calculated from the law of momentum conservation, which makes the detection of the photon unnecessary.

Recently a COLTRIMS detector has been used for an experimental study of single ionization of helium atoms by Compton scattering near the ionization threshold [10], i.e., for the study of reactions, where the energy transfer is close to the ionization potential of the helium atom $I_p = 24.6$ eV. The experiment has been carried out with 2.1 keV photons. As a result, a distinct difference between the cross section of a photon scattering at a free electron (given by the Thomson differential cross section) and the cross section of a bound electron was observed. The most remarkable difference of these distributions was observed exactly for rather small (several keV) photon energies. The largest values of the differential cross section were observed for the photon scattering angle close to π, i.e., for backscattering. However, this result has been already predicted by theoretical models of Compton ionization.

The present paper is motivated by new experiments on double ionization of helium by Compton scattering [14] utilizing the COLTRIMS technique to obtain differential cross sections, which thus go much beyond previous experiments reporting only total double ionization cross sections [11–13]. In this case it was possible to measure the momenta of a slow electron (with energies of several eV), and of the He^{++} ion. The kinetic energy of the ion is negligibly small due to its huge mass even for a photon energy of several tens of keV, so that it can be neglected in the energy balance of the process. In the experiments under consideration the momenta of the scattered photon and of the second electron are not measured. For the case of fairly large photon scattering angles this undetected second electron carries a large momentum, which it received from binary collision with the photon. Therefore, it is impossible to directly associate the momentum of the He^{++} ion with the momentum of the scattered photon. The coincidence method is used only for detecting the ion and a slow electron. Thus, the question arises, if it is possible, in this situation, to get information about the initial state correlations of the electron pair in the target atom, which is emitted in the ionization process? The present paper is devoted to answering this question.

The atomic units $\hbar = e = m_e = 1$ are used throughout the paper, unless stated otherwise. In these units, $c = 137$, $\alpha = 1/c = 1/137$, E(a.u.)=E(eV)/27.2, ω(a.u.)= 10^2 ω(keV)/2.72, the classical radius of the electron is $r_0 = \alpha^2$, $r_0^2 = 7.94 \cdot 10^{-26}$ cm^2, $r_0^2/(2\pi)^6 = 1.3 \cdot 10^{-30}$ cm^2 $= 1.3 \cdot 10^{-6}$ barn $= 0.46 \cdot 10^{-13}$ a.u.

2. Theory

2.1. Definitions

Let $\omega_1(\vec{k}_1)$ denote the energy (momentum) of the initial photon. In the experiment under consideration $\omega_1 = k_1 c = 40$ keV ($k_1 = 10.7$ a.u.). We choose $\vec{k}_1$ as the z-axis. The energy (momentum) of the scattered photon is denoted by $\omega_2(\vec{k}_2)$, and $\vec{Q} = \vec{k}_1 - \vec{k}_2$ is the momentum transfer. The linear polarizations of the photons $\vec{e}_1$, $\vec{e}_2$ satisfy the conditions $(\vec{e}_1 \cdot \vec{k}_1) = (\vec{e}_2 \cdot \vec{k}_2) = 0$. The momenta of the emitted electrons are denoted by $\vec{p}_1$, $\vec{p}_2$, $\vec{K}$ is the momentum of the residual He^{++} ion. In the non-relativistic case $E_j = p_j^2/2$ is the electron energy, $K^2/2M$ is the energy of the ion, which we neglect in the calculations, and $\varepsilon_0 = -79$ eV is the helium binding energy.

2.2. General formulas

Let us write down the Schrödinger equation for the helium atom interacting with the electromagnetic field $\vec{A}$:

$$i\frac{\partial}{\partial t}\Psi(\vec{r}_1,\vec{r}_2,\vec{r}_n,t) = \left[\frac{1}{2}\left(-i\vec{\nabla}_1 + \frac{1}{c}\vec{A}(\vec{r}_1,t)\right)^2 + \frac{1}{2}\left(-i\vec{\nabla}_2 + \frac{1}{c}\vec{A}(\vec{r}_2,t)\right)^2 + \frac{1}{8M}\left(-i\vec{\nabla}_n - 2\frac{1}{c}\vec{A}(\vec{r}_n,t)\right)^2 - \frac{2}{|\vec{r}_n-\vec{r}_1|} - \frac{2}{|\vec{r}_n-\vec{r}_2|} + \frac{1}{|\vec{r}_1-\vec{r}_2|}\right] \Psi(\vec{r}_1,\vec{r}_2,\vec{r}_n,t). \quad (1)$$

In Eq. (1) $M = 1836$ a.u. is the proton mass, $\vec{r}_n$ is the coordinate of the nucleus, and $\vec{r}_{1,2}$ denote the coordinates of the electrons. We choose the vector-potential in the following form:

$$\frac{1}{c}\vec{A}(\vec{r},t) = \sqrt{\frac{2\pi}{\omega_1}}\ \vec{e}_1\ e^{i(\vec{k}_1\vec{r}-\omega_1 t)} + \sqrt{\frac{2\pi}{\omega_2}}\ \vec{e}_2\ e^{-i(\vec{k}_2\vec{r}-\omega_2 t)} + (c.c.). \quad (2)$$

This choice of the vector-potential corresponds to the normalization of the photon wave function to one photon per unit volume and allows one to describe processes with one absorbed and one emitted photon. We remind the reader that $(\vec{k}_i \cdot \vec{e}_i) = 0$, and the relation $\mathrm{div}\vec{A}(\vec{r},t) = 0$ is fulfilled, which corresponds to the Coulomb gauge.

The interaction potential of an electron with the field is written as:

$$V_{int} = -i\frac{1}{c}\ (\vec{A}(\vec{r},t)\cdot\vec{\nabla}_r) + \frac{1}{2c^2}A^2(\vec{r},t) =$$

$$-i\left(\sqrt{\frac{2\pi}{\omega_1}}\ e^{i(\vec{k}_1\vec{r}-\omega_1 t)}(\vec{e}_1\cdot\vec{\nabla}_r) + \sqrt{\frac{2\pi}{\omega_2}}\ e^{-i(\vec{k}_2\vec{r}-\omega_2 t)}(\vec{e}_2\cdot\vec{\nabla}_r)\right) + (3.1)$$

$$\left(\frac{\pi}{\omega_1}\ (1 + e^{2i(\vec{k}_1\vec{r}-\omega_1 t)}) + \frac{\pi}{\omega_2}\ (1 + e^{-2i(\vec{k}_2\vec{r}-\omega_2 t)})\right) + (3.2)$$

$$\left(\frac{2\pi}{\sqrt{\omega_1\omega_2}}\ (\vec{e}_1\cdot\vec{e}_2)\ e^{i[(\vec{k}_1-\vec{k}_2)\vec{r}-(\omega_1-\omega_2)t]}\right) + c.c. \quad (3.3)$$

Equation (3.3) is the well-known Kramers-Heisenberg-Waller term [16,17], which gives the so-called A^2 approximation in the theory of Compton scattering. It is this term that we consider as the perturbation, which defines the matrix element M of the Compton ionization to be found. The terms in Eq. (3.1) describe the consecutive absorption and emission of a photon by an electron via the intermediate Green's function of the atom. We will not consider these interaction terms here, because they are rather small for the relatively high photon energy. They have been discussed in detail in recent paper [18]. Both these processes are of the second order in $\vec{A}$. However, as we will see below, the form of

the matrix element M corresponds to the first Born approximation in the case of the atom ionization by a charged particle, whereas the summands in Eq. (3.1) make up the second Born approximation.

The fully differential cross section (FDCS) of the double Compton ionization process can be written in the form:

$$d^{12}\sigma = \frac{(2\pi)^2\alpha}{\omega_1\omega_2}|M|^2\ (2\pi)^4\delta\left(\omega_1+\varepsilon_0-\omega_2-p_1^2/2-p_2^2/2\right) \times\delta^3\left(\vec{k}_1-\vec{k}_2-\vec{p}_1-\vec{p}_2-\vec{K}\right) \times\frac{d^3k_2}{(2\pi)^3}\frac{d^3p_1}{(2\pi)^3}\frac{d^3p_2}{(2\pi)^3}\frac{d^3K}{(2\pi)^3}. \quad (4)$$

As we have explained in the Introduction, only a slow electron and the He^{++} ion are detected in the experimental setup. Therefore, we have to integrate this expression with respect to $\vec{k}_1$ and $\vec{p}_1$ to get the sixfold differential cross section (6DCS). We obtain

$$\frac{d^6\sigma}{d^3p_2\ d^3K} = \frac{\alpha^2}{(2\pi)^6\omega_1^2}\int\frac{d^3k_2}{k_2}\ |M(\vec{k}-\vec{k}_1-\vec{p}_2-\vec{K},\vec{p}_2;\ \vec{k},\vec{k}_1)|^2$$

$$\times\delta\left(t-\frac{k_2}{k_1}-\frac{\alpha}{2k_1}(\vec{k}_1-\vec{k}_2-\vec{p}_2-\vec{K})^2\right),\quad t=1-\frac{E_2-\varepsilon_0}{\omega}\approx 1. \quad (5)$$

Here $\vec{k}_1-\vec{k}_2-\vec{p}_2-\vec{K}=\vec{p}_1$ stands for the momentum of electron 1. The δ-function takes energy conservation into account. We define $x,\ 0\le x\le 1$ by the relation $k_1=kx$ and rewrite Eq. (5) as follows:

$$\frac{d^6\sigma}{d^3p_2\ d^3K} = \frac{\alpha^4}{(2\pi)^6}\int_0^1 xdx\int d\Omega_2\ |M(\vec{k}_1-\vec{k}_2-\vec{p}_2-\vec{K}, p_2,\vec{K};\ \vec{k}_1,\vec{k}_2)|^2 \times\delta\left(t-x-\frac{\alpha k_1}{2}\left(\vec{n}_1-\vec{n}_2x-\frac{\vec{p}_2+\vec{K}}{k_1}\right)^2\right). \quad (6)$$

In Eq. (6) $\vec{n}_1$ ($\vec{n}_2$) is the unit vector directed along the vector $\vec{k}_1$ ($\vec{k}_2$).

Next, we consider the expression in the argument of the δ-function. First, we note that, with high accuracy, $t=1$, and $\alpha k_1/2\approx 0.04$. For photon backscattering, the contribution of the expression in the round brackets in the δ-function is about 16%, if $|\vec{p}_2+\vec{K}|\ll k$. An approximate solution of the equation for x to the first order in α is $x_1\approx 1-\frac{\alpha k_1}{2}(\vec{n}_1-\vec{n}_2-\frac{\vec{p}_2+\vec{K}}{k_1})^2$. This means that the energy of the final photon is very close to the energy of the initial one. Thus,

$$\frac{d^6\sigma}{d^3p_2\ d^3K} = \frac{\alpha^4}{(2\pi)^6}\int d\Omega_1\ x_1\ |M(\vec{k}_1-\vec{k}_2-\vec{p}_2-\vec{K},\vec{p}_2,\vec{K};\ \vec{k}_1,\vec{k}_2)|^2, \quad (7)$$

where we have put $\vec{k}_2=kx_1\vec{n}_2$.

Now we know the momenta of both electrons: $\vec{p}_1\approx k_1(\vec{n}_1-x_1\vec{n}_2)-\vec{p}_2-\vec{K}$ and $\vec{p}_2$. If the momentum $\vec{p}_2$ of electron 2, which we measure, is small and known, the momentum of the other electron, $\vec{p}_1$, with respect to which we integrate, can be both small and large depending on the momentum transfer Q. When we integrate with respect to the scattering photon angle θ, the value p_1 changes considerably.

Within the A^2 model we have

$$M(\vec{p}_1,\vec{p}_2;\vec{e}_1,\vec{e}_2)=(\vec{e}_1\cdot\vec{e}_2)\langle\Phi^-(\vec{p}_1,\vec{p}_2)|e^{i(\vec{k}_1-\vec{k}_2)\cdot\vec{r}_1}+e^{i(\vec{k}_1-\vec{k}_2)\cdot\vec{r}_2}|\Phi_0\rangle. \quad (8)$$

If the momentum transfer Q is fairly large, the momenta of the two electrons are quite different. This kinematical condition is very close to the above mentioned EMS geometry, where the two final electrons (the incident one and the fast ejected one) approximately share the initial energy, and their scattering angles are about 45°. In this case the momentum transfer is maximal. But the third ejected electron can be slow, and its production mechanism is mainly shake-off. It was shown in [5] that this kinematics is the best one to observe the correlations by measuring the angular distributions of the final fragments.

To get the final formulas we choose the final state orthogonal to the initial one:

$$\langle\tilde{\Phi}^-(\vec{p}_1,\vec{p}_2)|=\langle\Phi^-(\vec{p}_1,\vec{p}_2)|-\langle\Phi^-(\vec{p}_1,\vec{p}_2)|\Phi_0\rangle\langle\Phi_0|, \quad (9)$$

and take into account the symmetrization by introducing the factor $1/\sqrt{2}$. The summation/averaging over the final and initial photon polarizations gives the factor $[1+(\vec{n}_1\cdot\vec{n}_2)^2]$ in the integrand in Eq. (7). Finally we obtain

$$6DCS\equiv\frac{d^6\sigma}{d^3p_2\ d^3\ K} = \frac{r_0^2}{(2\pi)^6}\int d^2n_2\ x_1[1+(\vec{n}_1\cdot\vec{n}_2)^2] \times\Big|\langle\Phi^-(\vec{p}_1,\vec{p}_2)|e^{i\vec{Q}\cdot\vec{r}_1}|\Phi_0\rangle$$

$$+\langle\Phi^-(\vec{p}_1,\vec{p}_2)|e^{i\vec{Q}\cdot\vec{r}_2}|\Phi_0\rangle-2\langle\Phi^-(\vec{p}_1,\vec{p}_2)|\Phi_0\rangle\langle\Phi_0|e^{i\vec{Q}\cdot\vec{r}}|\Phi_0\rangle\Big|^2. \quad (10)$$

In the integrands the variable p_1 is linked to the variable r_1. Therefore, the first term in Eq. (10) describes the direct process, the second one corresponds to the exchange process, and the third term appears due to the orthogonalization. Explicitly, we denote these terms as

$$T_1=\langle\Phi^-(\vec{p}_1,\vec{p}_2)|e^{i\vec{Q}\cdot\vec{r}_1}|\Phi_0\rangle,\quad T_2=\langle\Phi^-(\vec{p}_1,\vec{p}_2)|e^{i\vec{Q}\cdot\vec{r}_2}|\Phi_0\rangle,$$

$$T_3=2\langle\Phi^-(\vec{p}_1,\vec{p}_2)|\Phi_0\rangle\langle\Phi_0|e^{i\vec{Q}\cdot\vec{r}}|\Phi_0\rangle.$$

We also remind the reader that $x_1=1-(\alpha/2k_1)(k_1(\vec{n}_1-\vec{n}_2)-\vec{p}_2-\vec{K})^2$, $\vec{Q}=\vec{k}_1-\vec{k}_2=k_1(\vec{n}_1-x_1\vec{n}_2)$, and $\vec{p}_1=\vec{Q}-\vec{p}_2-\vec{K}$.

2.3. Physical considerations

Now let us consider in more detail the physical mechanisms that control the Compton double ionization. Above we have introduced the notions of the "fast" electron (the undetected one) labeled by the index 1 and the "slow" electron, which we detect and label by the index 2. To give a clearer physical picture, we use two types of description of the initial helium ground state: a simple Hylleraas (HY) helium wave function ($I_p^{Hy}=2.85au$)

$$\Phi_0^{Hy}(\vec{r}_1,\vec{r}_2)=\frac{Z^3}{\pi}\ e^{-Z(r_1+r_2)},\quad Z=27/16,$$

and a highly correlated ground state wave function CF [23] (see Appendix). We describe the final state (which consist of two electrons and one doubly charged ion) by either taking a plane wave (PW) for the "fast" electron and the Coulomb wave (CW)($Z=2$) for the slow electron, or the well known 3C double continuum wave function [24].

For discussing the physics it is instructive to go to the simplest Hy+PW+CW model since this provides analytical expressions for the matrix elements T_j and allows one to give them a clear physical interpretation. Recall that, after the symmetrization, the matrix elements T_j are presented in such a way that the momentum of the fast electron $\vec{p}_1$ mates the coordinate $\vec{r}_1$. In the matrix element T_1 the momenta $\vec{Q}$ and $\vec{p}_1$ form the combination $\vec{Q}-\vec{p}_1=\vec{p}_2+\vec{K}$ in the exponential, i.e., here the total momentum in the exponential is small. By varying this momentum and measuring it, we

probe the momentum distribution of the active electron with coordinate $\vec{r}_1$. This term corresponds to the direct interaction of a photon with an electron. The electron both absorbs the photon and emits it. The second ("slow") electron is emitted with momentum $\vec{p}_2$ due to the shake-off mechanism. The term T_1 gives the most valuable information about the internal structure of the atom, in full analogy to $(e, 3e)$ ionization. This term does not depend on the photon scattering angle θ, and its integration in Eq. (10) does not change it.

Now, we turn to the term T_2. Here, the fast momenta $\vec{Q}$ and $\vec{p}_1$ no longer meet each other and enter different integrals over the coordinates. Their contributions quickly vanish with increasing photon scattering angle resulting in larger momentum transfers Q. In the matrix element T_2, the momenta form the combination $\vec{Q} - \vec{p}_2$ in the exponential. At large scattering angles of the photon, the momentum transfer increases rapidly, and this term rapidly tends to zero. Here the physics can be interpreted as follows. Electron 2 absorbs the photon and transfers the absorbed momentum to electron 1 through the internal *ee*-correlation. Electron 1 escapes with the momentum $\vec{p}_1$. This is a typical exchange process, and if there are no correlations of electrons in the atom, even through the mean field, this term is equal to zero.

The matrix element T_3 is artificial, because it arises due to the non-orthogonality of the trial wave functions of the initial and final states of the helium atom, and, in the Hy+PW+CW model, does not depend at all on the angles of the electron and the ion. Usually, it is small in the entire range of photon scattering angles.

2.4. Numerical implementation

To obtain theoretical values of the cross sections we have to calculate multiple integrals. In Eq. (10) there is also a double integral. The matrix elements in Eq. (10) are at least triple integrals (depending on the model). The details of the analytical evaluation of integrals for the model CF+3C are given in the Appendix.

For the numerical integrations we used a globally adaptive subdivision scheme [19]. The inner integrations have been performed with an absolute accuracy of 10^{-4} using the code DCUHRE [20], while the outer integrations have been calculated with a relative accuracy of 10^{-2} using the code CUHRE [21] (note that DCUHRE and CUHRE are similar codes, but CUHRE works only on Linux systems). The calculations were performed at the Central Information and Computer Complex and heterogeneous computing platform HybriLIT using the supercomputer "Govorun" of the Joint Institute for Nuclear Research (JINR).

3. Results and discussion

In Ref. [14], the single differential cross sections were calculated by further integration of Eq. (10). Despite the fact that even in this case some differences were noted in the behavior of single differential cross sections depending on the choice of a pair of model wave functions of the initial and final states of the helium atom, such cross sections still do not give direct information on the electronic correlations in the target, which can be obtained by examining, for example, $(e, 3e)$ ionization in the quasielastic impact kinematics [5,6].

From the viewpoint of the theory, fully differential studies of Compton double ionization would have major advantages over $(e, 3e)$ and ion induced reactions as a new method of dynamic spectroscopy of atoms. The advantages include, first, the dominance of the "first Born approximation" (5), which now does not directly depend on either the initial photon energy or Q^2 in the denominator of matrix element (10), as it is for charged particle impact. Second, the second Born term (see, for example, [15]) contains the energy of the initial photon in the denominator of Green's function and can be small enough. Currently these advantages cannot be fully exploited because, due to the extremely small cross sections, fully differential experiments are not feasible today. The current best experiments using the COLTRIMS technique leaves the momentum transfer unobserved, requiring theory to integrate over this observable. The detected events thus contain also events at small momentum transfers Q, which significantly hampers the interpretation. Let us consider this point in more detail.

As mentioned above, the integration in Eq. (10) does not affect the term T_1, because it does not depend on the momentum transfer explicitly (at least in the Hy+PW+CW model). The result of the integration of the other terms is non-trivial, but the main contribution to integral (10) comes from the integration over the forward scattering cone of the photon. This conclusion is confirmed by a more detailed study of the integrand in Eq. (10). As the scattering angle increases, the asymmetry in the energies of the electrons also increases, the terms T_2 and T_3 decrease rapidly, whereas the matrix element T_1 survives and, as it was explained above, it carries the most valuable spectroscopic information on the distribution of momenta of the pair of electrons in the atom.

Here we consider several examples. First, let us put $\vec{p}_2 + \vec{K} = 0$. This is the so-called Bethe ridge, where T_1 is maximal, and the He^+ ion remains at rest. In this case, the maximal value of Q is about $Q_{\max} = 2k \approx p_1^{\max} \approx 20$, and the maximal non-relativistic electron kinetic energy $E_1 = p_1^2/2$ is about 5.4 keV. It is interesting to note that its relativistic analogue $E_1^{kin} = c^2[\sqrt{1 + p_1^2/c^2} - 1] \approx 5.4$ keV. The difference is in the second digit, which confirms the validity of the non-relativistic approach.

We introduce the vector $\vec{u} = \vec{p}_2 + \vec{K}$ and choose the geometry, where the vectors $\vec{p}_2,\ \vec{K},\ \vec{u}$ are collinear, i.e., $u = |\vec{p}_2 + \vec{K}| = |p_2 - K|$. We begin the calculations from $u = 0$, where the initial point is $E_2^{(0)} = 20$ eV, and then increase E_2 up to 50 eV, keeping K fixed at $K = \sqrt{2E_2^{(0)}}$. In this case the 6DCS also depends on the angle χ, which is the emission angle of the second electron in the laboratory frame with respect to the light propagation axis, i.e., between the vectors $\vec{k}$ (z axis) and $\vec{p}_2$. We carry out the calculations for three emission angles, ranging from forward to backward emission: $\chi = 0^\circ,\ 90^\circ, 180^\circ$.

The 6DCS in the simplest model (Hy+PW+CW) for the geometry described above is presented in Figs. 1–3 the black squares show the contribution of only the term T_1, while the dashed red line corresponds to the sum of all three terms. The 6DCS for the angles of the emitted electrons $\chi = 0^\circ$ and $\chi = 180^\circ$ demonstrates that the contribution of the terms T_2 and T_3 practically vanishes for the chosen geometry and relatively high energies of the slow electron. On the contrary, for $\chi = 90^\circ$ we see a noticeable difference between the curves. We will explain this effect below.

In Figs. 4–6 we present the 6DCS for two models. The model CF+3C (see Appendix), which supposedly gives the best results of those shown in the Figures, is presented by the solid lines, the model CF+PW+CW ($\xi_1 = \xi_{12} = 0,\ \xi_2 = -2/p_2$, see Appendix for definition of ξ) is presented by the dashed lines for comparison. The black line corresponds to the term T_1 in (10) taken alone, the red line is the coherent sum of all the three terms. Even for sufficiently high energies of the "slow" electron, the differences in the behavior of the T_1 and $T_1 + T_2 + T_3$ curves are quite noticeable within the same model and indicate an essential influence of the $T_2 + T_3$ amplitudes, especially for the CF+PW+CW model with $\chi = 90^\circ$. We remind that T_1 is the amplitude mediated only by electron correlation, which is most important for correlation spectroscopy. $T_2 + T_3$ are the terms, where p_2 is the momentum of the primary electron from the Compton event. For small momentum transfer, both electrons have similar energy, thus, one loses the clear fingerprint of the electron correlation in the observed differential cross sections.

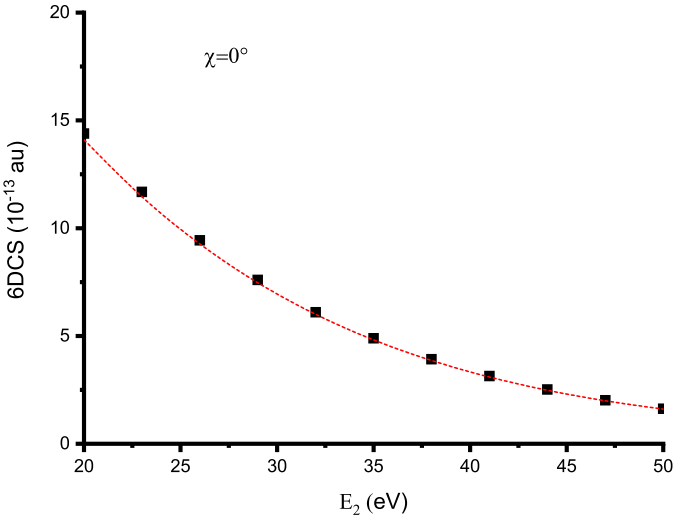

Fig. 1. The 6DCS for double ionization of He by Compton scattering at a photon energy of 40 keV as a function of the energy of one of the emitted electrons (labeled as electron 2 with the energy E_2). The model (PW+CW+Hy) uses a weakly correlated initial state, but a plane wave for electron 1 and a Coulomb wave for electron 2. The following geometry is selected: the emission angle of electron 2 with respect to the incoming photon direction $\chi = 0$, the ion momentum $\vec{K}$ and electron momentum $\vec{p}_2$ are collinear. Further description see in the text. Black squares: T_1 only; dashed red line: the sum of all three terms. (For interpretation of the references to colour in this figure legend, the reader is referred to the web version of this article.)

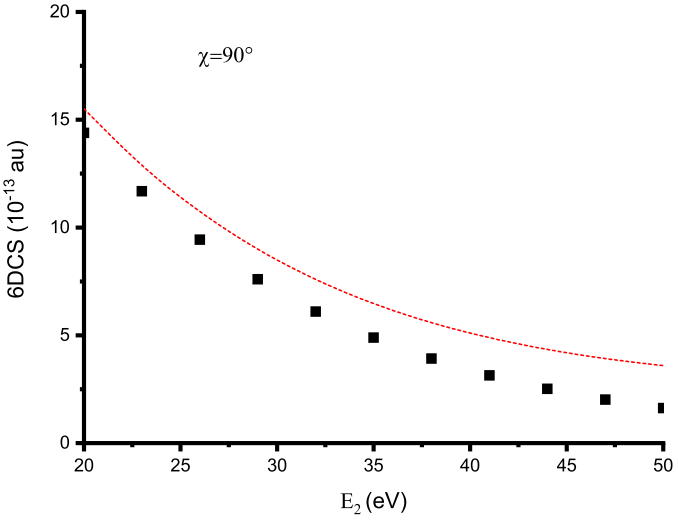

Fig. 2. The same as in Fig. 2 for the angle $\chi = 90^\circ$.

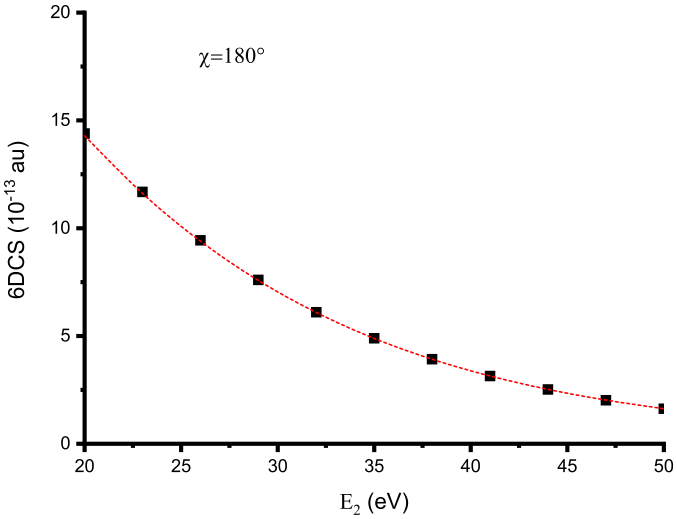

Fig. 3. The same as in Fig. 2 for the angle $\chi = 180^\circ$.

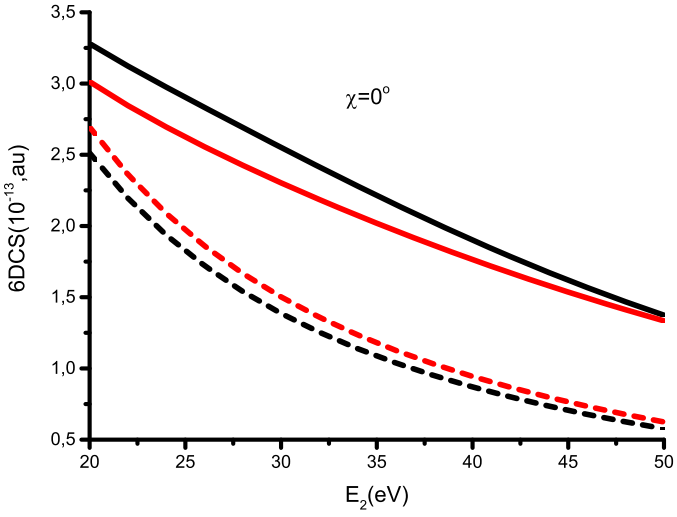

Fig. 4. The 6DCS for double ionization of He by Compton scattering at a photon energy of 40 keV as a function of the energy of one of the emitted electrons (labeled as electron 2 with energy E_2). The following geometry is selected: the emission angle of electron 2 with respect to the incoming photon direction $\chi = 0$, the ion momentum $\vec{K}$ and electron momentum p_2 are collinear. A further description see in the text. Solid lines: the best initial and final state wave function (3C+CF); dashes lines: the same highly correlated initial state but a plane wave for electron 1 and a Coulomb wave for electron 2 (PW+CW+CF). Black lines: T_1 only; red lines: the sum of all three terms (see Appendix I). (For interpretation of the references to colour in this figure legend, the reader is referred to the web version of this article.)

Let us shortly discuss the observed differences in the curves for all three considered models. The Hy ground state wave function gives the 6DCS about 10 times larger than that for the correlated CF wave function. However, the curves for the forward/backward emission of the "slow" electron demonstrate a negligible contribution of the terns T_2 and T_3. In the case of the CF wave function, for $\chi = 0^\circ$ and $\chi = 180^\circ$ we see a close relative behavior of the curves. However, there is a very big exception for $\chi = 90^\circ$. It can be explained as follows. Our division of the emitted electrons into "fast" and "slow" ones is rather arbitrary. It makes sense only in the region of sufficiently large angles θ, where the magnitudes of the momenta p_1 and p_2 differ significantly. At small scattering angles of the photon, these momenta are comparable. In this region, the momentum transfer $\vec{Q}$ is small and practically orthogonal to the initial photon momentum $\vec{k}$. The maximum of the matrix element T_2 is reached under the condition $\vec{Q} - \vec{p}_2 = 0$. In this case, the "slow" electron moves collinear with the momentum transfer, i.e., at the angle $\chi = 90^\circ$. Consequently, here the term T_2 seems to dominate, which explains the difference of the 6DCS for only T_1 term from that for the sum of all three terms at this angle. This is solely due to the fact that the forward scattering cone of the final photons vastly contributes to the 6DCS.

Thus, the question arises: is it possible to eliminate the negative effect of the events with the photon scattered into the forward cone, e.g., by integrating in Eq. (10) not from the photon scattering angle $\theta = 0$, but from a cutoff angle θ_0?

Such a situation is presented in Figs. 7 and 8. In all the cases, the initial states are described by the good CF trial function, and the curves are shown for different final state wave functions. The energy of the detected electron is $E_2 = 10$ eV, and a special momentum configuration $\vec{p}_2 + \vec{K} = 0$ is chosen again. What do we

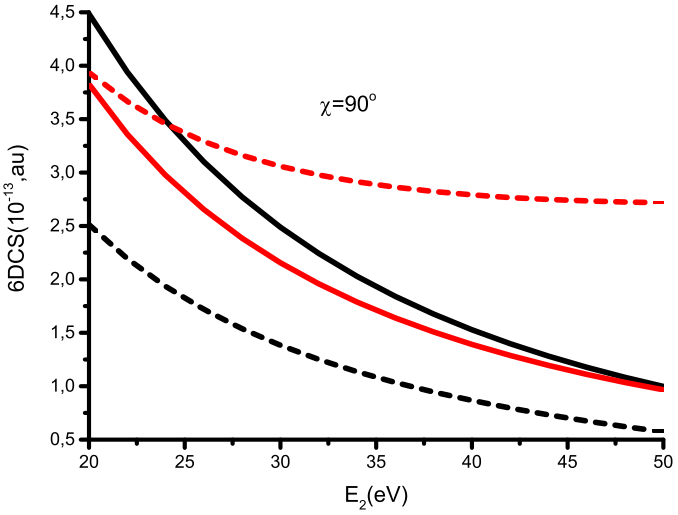

Fig. 5. The same as in Fig. 4 for the angle $\chi = 90^\circ$.

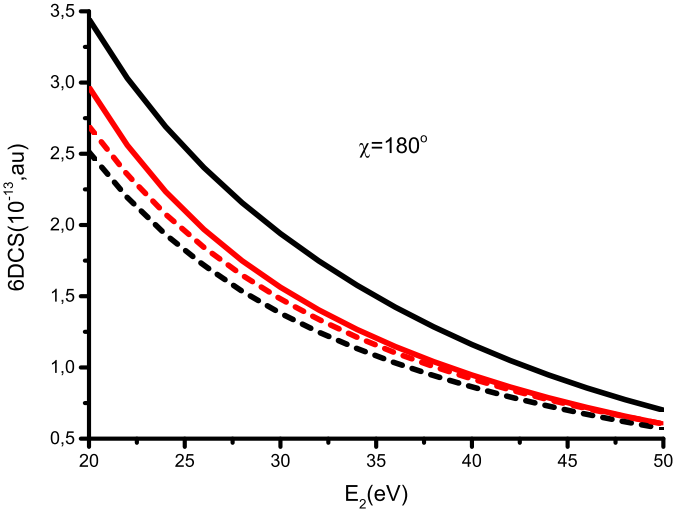

Fig. 6. The same as in Fig. 4 for the angle $\chi = 180^\circ$.

see in these Figures? Already for $\theta_0 = 20^\circ$, the contribution of the terms T_2 and T_3 is practically reduced to zero (recall that the photon energy $\omega = 40$ keV), and disappears completely for $\theta_0 = 40^\circ$. Moreover, in the case of a plane wave for the "fast" electron (model PW+CW+CF, dashed line), we observe a constant 6DCS. The constant 6DCS means the minimal dependence of the model on the final state, and we can concentrate on studying ee-correlations in the target.

The other final states show a dependence of the cross section on the scattering angle χ of the slow electron. We shortly describe these final states. Using the final state CW $(\xi_1 = -1/p_1)$+ CW$(\xi_2 = -2/p_2)$, we describe the "fast" electron by a Coulomb wave in the field of the residual ion He^+ $(Z = 1)$, while the "slow" electron "sees" the charge of the nucleus $Z = 2$. Such a function partially takes into account the final correlation of the electrons with different velocities. The final state CW $(\xi_1 = -2/p_1)$+ CW$(\xi_2 = -2/p_2)$ supposes the absence of correlations for the final electrons, and they both move in the field of the ion He^{++}. The BBK (3C) final wave function is described in the Appendix.

The dependence of these curves on the angle χ is different from the constant in the model PW+CW+CF, i.e., the final state plays a role here, but let us pay attention to the Y axis scale. As the cutoff angle increases, the 'fast' electron's energy grows drastically,

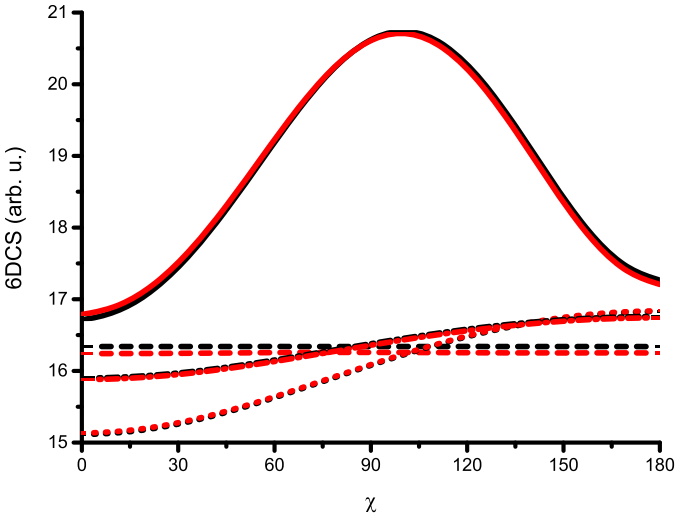

Fig. 7. The 6DCS Eq. (10) (arb.units) versus the emission angle χ of one of the electrons with respect to the incoming photon direction. The photon scattering angles $\theta < \theta_0 = 20^\circ$ are excluded, $E_2 = 10eV$, $\vec{p}_2 + \vec{K} = 0$ (Bethe ridge). Solid line: model 3C+CF, dashed line: model PW+CW+CF($\xi_2 = -2/p_2$), dashed-dotted line: model CW $(\xi_1 = -1/p_1)$+ CW$(\xi_2 = -2/p_2)$+CF, dotted line: CW$(\xi_1 = -2/p_1)$+ CW$(\xi_2 = -2/p_2)$+CF. Black lines: T_1, red lines: all three terms in (10). (For interpretation of the references to colour in this figure legend, the reader is referred to the web version of this article.)

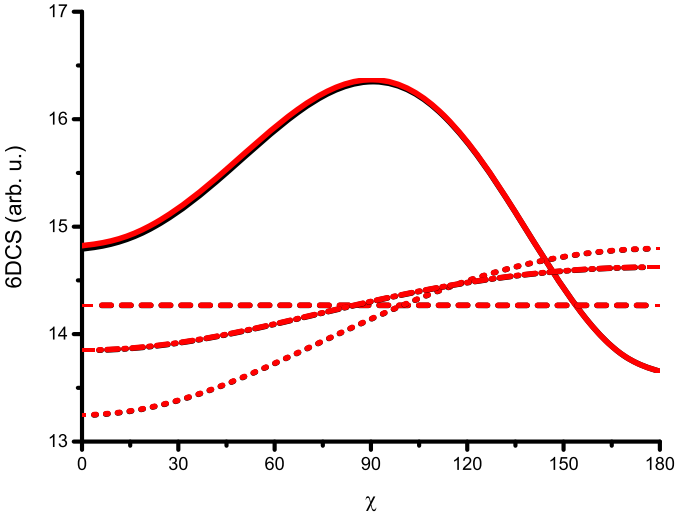

Fig. 8. The same as in Fig. 7 with the photon scattering angles $\theta < \theta_0 = 40^\circ$ excluded.

so that the curves tend to the dashed straight line, the deviation not exceeding 20% for $\theta_0 = 40^\circ$ even for the 3C model. This means that, when θ_0 increases, the wave function of the fast electron, whose momentum is closely related to the growing momentum transfer Q, tends increasingly to the plane wave limit. Although, it should be kept in mind that even at considerably high photon energies the Coulomb function approaches a plane wave very slowly.

However, the most important point in this scheme is that we get rid of the negative influence of the terms T_2 and T_3, and one can focus on the theoretical study of the term T_1. In this sense, Compton double ionization of the atom resembles a symmetric $(e, 3e)$ reaction with a large momentum transfer [5,6].

How could one filter out the events, for which the photon has been scattered at small forward angles? In principle, one could cover the small solid angles with a veto photon counter. For this purpose, no photon energy measurement would be necessary, but a high detection efficiency is essential for an effective veto. In prac-

tice, however, such a small angle veto is difficult to implement because of the required high intensity of the primary photon beam.

In practice, it is more promising to use a large area pixel detector DEPFET [25] at backward angles than a veto of small angle scattering. Such detectors can easily cover 10-20% solid angle, if placed in the backward scattering direction. Yet another technical option would be to measure the momenta of both electrons and the ion in coincidence. In this case the photon momentum transfer could be obtained from the law of momentum conservation, and this way the events with small momentum transfer could be excluded during the analysis.

4. Conclusions

The paper deals with the possibility of using the double ionization induced by Compton scattering as a method of dynamic spectroscopy of atoms and molecules. The theoretical study is motivated by recent experiments by the Goethe University Frankfurt experimental team, in which the momenta of the ion and of one of the ejected electrons were measured in coincidence without detecting the scattered photon [14]. The theoretical description of the process is based on the so-called A^2 approximation. The fully differential cross section of the process was derived by analytical evaluation and numerical calculations of multiple integrals. For a pair of strongly correlated initial and final states, the number of integrations was six, for which it was necessary to develop special numerical methods and to carry out a careful analytical analysis of the inner integrals.

It is shown that the double ionization driven by Compton scattering can be an effective method of dynamic spectroscopy only in the case, where it is possible to exclude the events with small momentum transfer from the consideration. The characteristics of these events, for which the photon is scattered in the forward cone and the energies of both electrons are rather small and comparable with each other, are influenced by the exchange processes that cannot be excluded and hinder obtaining direct information about the electron correlations in the target bound state. Two possible ways to meet that challenge experimentally would be either to measure both electrons and the ion in coincidence or to place a large area photon detector with 20% solid angle at backward direction.

Declaration of Competing Interest

The authors declare that they have no known competing financial interests or personal relationships that could have appeared to influence the work reported in this paper.

CRediT authorship contribution statement

O. Chuluunbaatar: Software, Visualization. **S. Houamer:** Software, Visualization. **Yu.V. Popov:** Conceptualization, Supervision, Writing – original draft. **I.P. Volobuev:** Conceptualization, Writing – review & editing. **M. Kircher:** Conceptualization, Writing – review & editing. **R. Dörner:** Conceptualization, Writing – review & editing.

Acknowledgements

The calculations were performed on the basis of a heterogeneous computing platform HybriLIT on supercomputer "Govorun" (LIT, Joint Institute of Nuclear Research). The work was partially supported by the Hulubei-Meshcheryakov JINR programs, the Heisenberg-Landau program, grant of RFBR and MECSS No. 20-51-4400, grant of Foundation of Science and Technology of Mongolia SST 18/2018, grant of the RFBR No. 19-02-00014a. S.H. thanks the DGRSDT-Algeria Foundation for support. R.D. and M.K. acknowledge funding by Deutsche Forschungsgemeinschaft (DFG).

Appendix A. 3C + correlated initial state

To estimate the ability of this method to study (*ee*)-correlations in the target atom, we use the correlated final BBK (3C) wave function and a highly correlated trial initial state, normalized to 1 [23], which we denote as CF:

$$\Phi_0^{CF}(\vec{r}_1,\vec{r}_2)=\sum_{j=1}^{10} D_j(\mathrm{e}^{-a_j r_1-b_j r_2}+\mathrm{e}^{-a_j r_2-b_j r_1})\mathrm{e}^{-\gamma_j r_{12}}. \tag{A1}$$

This function provides the helium ground state energy $\varepsilon_0^{CF}=-2.90371$ a.u., which is practically equal to its experimental value $\varepsilon_0^{\exp}=-2.903724$ a.u. The final double continuum wave function is given by the well-known BBK (3C) function [24]:

$$\Phi_{3C}^{(-)}(\vec{r}_1,\vec{r}_2)=\mathrm{e}^{\mathrm{i}\vec{p}_{12}\cdot\vec{r}_{12}}\phi_1^{-*}\phi_2^{-*}\phi_{12}^{-*}. \tag{A2}$$

Here

$$\phi_j^{-*}(\vec{p}_j,\vec{r})=R(\xi_j)e^{-\mathrm{i}\vec{p}_j\vec{r}}{}_1F_1[-\mathrm{i}\xi_j,1;\mathrm{i}(p_j r+\vec{p}_j\cdot\vec{r})],$$

with

$$\vec{p}_{12}=\frac{1}{2}(\vec{p}_1-\vec{p}_2);\quad \xi_{12}=\frac{1}{2p_{12}};\quad \xi_j=-\frac{2}{p_j}\ (j=1,2);$$

$$R(\xi)=e^{-\pi\xi/2}\ \Gamma(1+\mathrm{i}\xi).$$

We write each matrix element in Eq. (10) in the following form

$$\begin{aligned}
&T_1\left(\vec{p}_1,\vec{p}_2;\vec{Q}\right)\\
&=\langle\Phi^-\left(\vec{p}_1,\vec{p}_2\right)\left|e^{i\vec{Q}\cdot\vec{r}_1}\right|\Phi_0\rangle\\
&=-\sum_{j=1}^{10} D_j\int\frac{d^3p}{(2\pi)^3}\ \frac{\partial}{\partial\gamma_j}I_{12}\left(\vec{p}+\vec{p}_{12},\vec{p}_{12};\gamma_j\right)\\
&\times\left[\frac{\partial}{\partial a_j}I_1\left(\vec{Q}-\vec{p},\vec{p}_1;a_j\right)\ \frac{\partial}{\partial b_j}I_2\left(\vec{p},\vec{p}_2;b_j\right)+\left(a_j\rightleftarrows b_j\right)\right],
\end{aligned} \tag{A3.1}$$

$$\begin{aligned}
&T_2(\vec{p}_1,\vec{p}_2;\vec{Q})\\
&=\langle\Phi^-(\vec{p}_1,\vec{p}_2)|e^{\mathrm{i}\vec{Q}\cdot\vec{r}_2}|\Phi_0\rangle\\
&=-\sum_{j=1}^{10} D_j\int\frac{d^3p}{(2\pi)^3}\ \frac{\partial}{\partial\gamma_j}I_{12}(\vec{p}+\vec{p}_{12},\vec{p}_{12};\gamma_j)\\
&\times\left[\frac{\partial}{\partial a_j}I_1(-\vec{p},\vec{p}_1;a_j)\ \frac{\partial}{\partial b_j}I_2(\vec{p}+\vec{Q},\vec{p}_2;b_j)+(a_j\rightleftarrows b_j)\right],
\end{aligned} \tag{A3.2}$$

and

$$\begin{aligned}
&T_3(\vec{p}_1,\vec{p}_2;\vec{Q})\\
&=\langle\Phi^-(\vec{p}_1,\vec{p}_2)|\Phi_0\rangle\\
&=-\sum_{j=1}^{10} D_j\int\frac{d^3p}{(2\pi)^3}\ \frac{\partial}{\partial\gamma_j}I_{12}(\vec{p}+\vec{p}_{12},\vec{p}_{12};\gamma_j)\\
&\times\left[\frac{\partial}{\partial a_j}I_1(-\vec{p},\vec{p}_1;a_j)\ \frac{\partial}{\partial b_j}I_2(\vec{p},\vec{p}_2;b_j)+(a_j\rightleftarrows b_j)\right].
\end{aligned} \tag{A3.3}$$

In Eq. (A3) the functions $I_s(\vec{p},\vec{p}_s;\lambda)$, where the (multi)index $s=1,2,12,$ are given by

$$\begin{aligned}
I_s(\vec{p},\vec{p}_s;\lambda)&=\int\frac{d^3r}{r}\ \phi_s^{-*}(\vec{p}_s,\vec{r})\ e^{-\lambda r+i\vec{p}\cdot\vec{r}}\\
&=4\pi\ R(\xi_s)\frac{[(\lambda-ip_s)^2+p^2]^{i\xi_s}}{[(\vec{p}-\vec{p}_s)^2+\lambda^2]^{(1+i\xi_s)}}.
\end{aligned} \tag{A4}$$

Now we can write the 6DCS in the following form:

$$\frac{d^6\sigma}{d^3p_2\ d^3K} = \frac{r_0^2}{(2\pi)^6}\int_0^{2\pi} d\phi \int_0^{\pi} \sin\theta d\theta\ x_1[1+(\vec{n}\cdot\vec{n}_1)^2] \times \left|T_1+T_2-2\langle\Phi_0|e^{i\vec{Q}\cdot\vec{r}}|\Phi_0\rangle T_3\right|^2. \quad (A5)$$

For definiteness, in Eq. (A5) we choose the following signatures of the vectors:

$$\vec{k} = k(0,0,1), \quad \vec{p}_2 = p_2(\sin\chi, 0, \cos\chi),$$
$$\vec{k}_1 = kx_1(\sin\theta\cos\phi, \sin\theta\sin\phi, \cos\theta)$$

From Eq. (A3) we can get various models of the final states:

1. $\xi_1 = \xi_{12} = 0$. It is the plane wave (PW) approximation for the invisible electron.
2. $\xi_1 = -2/p_1,\ \xi_{12} = 0$. Here we have the product of two Coulomb waves with $Z = 2$.
3. $\xi_1 = -1/p_1,\ \xi_{12} = 0$. If the outgoing invisible electron is fast, it sees the charge +1 of the ion He^+. It is a weak final correlation for two nonsymmetric final electrons.

Some details of numerical calculations. Let us consider the following 6D integral:

$$R(\vec{y};\vec{\eta};\vec{k};a;b;c;\xi) \equiv R =$$

$$\int d^3r_1 \int d^3r_2 e^{-i\vec{y}\vec{r}_1 - i\vec{\eta}\vec{r}_2} e^{-i\vec{k}\vec{r}_2} e^{-ar_1-br_2-cr_{12}} \times {}_1F_1\left(-i\xi, 1; ikr_2 + i\vec{k}\vec{r}_2\right), \quad (A6)$$

where $a,\ b,\ c > 0$, and we assume that $Re(-i\xi) > 0$. Using the integral representation of the confluent hypergeometric function and the Fourier transform of $e^{-cr_{12}}$, one can easily perform the integration with respect to the spatial coordinates. We get

$$R = \frac{8}{\Gamma(1+i\xi)\Gamma(-i\xi)} \frac{\partial^3}{\partial a\partial b\partial c} \int_0^1 dt t^{-i\xi-1}(1-t)^{i\xi} I(t), \quad (A7)$$

and

$$I(t) = \int d\vec{p} \frac{1}{c^2+p^2} \frac{1}{a^2+(-\vec{y}-\vec{p})^2} \frac{1}{(b-itk)^2+(\vec{\eta}+\vec{k}-t\vec{k}-\vec{p})^2}. \quad (A8)$$

Integral (A8) may be written in the following form Lewis et al. [22]:

$$I(t) = 2\pi^2 \int_0^{\infty} \frac{du}{([\alpha_1-\alpha_0]t+\alpha_0)u^2 + 2([\beta_1-\beta_0]t+\beta_0)u + [\gamma_1-\gamma_0]t+\gamma_0}$$

$$= 2\pi^2 \int_0^{\infty} \frac{du}{\alpha_0u^2+2\beta_0u+\gamma_0} \times \left(1+\frac{(\alpha_1-\alpha_0)u^2+2(\beta_1-\beta_0)u+\gamma_1-\gamma_0}{\alpha_0u^2+2\beta_0u+\gamma_0}t\right)^{-1}, \quad (A9)$$

where

$$\alpha_0 = (\vec{\eta}+\vec{k}+\vec{y})^2 + (a+b)^2, \quad \alpha_1 = (\vec{\eta}+\vec{y})^2 + (a+b-ik)^2,$$
$$\beta_0 = c[(\vec{\eta}+\vec{k}+\vec{y})^2 + (a+b)^2] + b(y^2+a^2+c^2) + a((\vec{\eta}+\vec{k})^2+b^2+c^2),$$
$$\beta_1 = c[(\vec{\eta}+\vec{y})^2 + (a+b-ik)^2] + (b-ik)(y^2+a^2+c^2) + a(\eta^2+(b-ik)^2+c^2),$$
$$\gamma_0 = (y^2+(a+c)^2)((\vec{\eta}+\vec{k})^2+(b+c)^2),$$
$$\gamma_1 = (y^2+(a+c)^2)(\eta^2+(b-ik+c)^2).$$

Substituting (A9) into (A7) and using the integral representation of the hypergeometric function, we obtain the following chain of transformations:

$$R = -16\pi^2 \frac{\partial^3}{\partial a\partial b\partial c} \int_0^{\infty} \frac{du}{\alpha_0u^2+2\beta_0u+\gamma_0} \times {}_2F_1\left(1, -i\xi; 1, -\frac{(\alpha_1-\alpha_0)u^2+2(\beta_1-\beta_0)u+\gamma_1-\gamma_0}{\alpha_0u^2+2\beta_0u+\gamma_0}\right)$$

$$= -16\pi^2 \frac{\partial^3}{\partial a\partial b\partial c} \int_0^{\infty} \frac{du}{\alpha_0u^2+2\beta_0u+\gamma_0} \times \left(1+\frac{(\alpha_1-\alpha_0)u^2+2(\beta_1-\beta_0)u+\gamma_1-\gamma_0}{\alpha_0u^2+2\beta_0u+\gamma_0}\right)^{i\xi}$$

$$= -16\pi^2 \frac{\partial^3}{\partial a\partial b\partial c} \int_0^{\infty} \frac{du}{\alpha_0u^2+2\beta_0u+\gamma_0} \left(\frac{\alpha_1u^2+2\beta_1u+\gamma_1}{\alpha_0u^2+2\beta_0u+\gamma_0}\right)^{i\xi}$$

Making the change of variables $u = x/(1-x)$, finally we obtain:

$$R(\vec{y};\vec{\eta};\vec{k};a;b;c;\xi) = -(4\pi)^2 \frac{\partial^3}{\partial a\partial b\partial c} \int_0^1 \frac{dx}{\alpha_0x^2+2\beta_0x(1-x)+\gamma_0(1-x)^2} \times \left(\frac{\alpha_1x^2+2\beta_1x(1-x)+\gamma_1(1-x)^2}{\alpha_0x^2+2\beta_0x(1-x)+\gamma_0(1-x)^2}\right)^{i\xi}. \quad (A10)$$

References

[1] Chuluunbaatar O, Houamer H, Popov YV, Volobuev IP, Kircher M, Doerner R. Compton ionization of atoms as a method of dynamical spectroscopy. J Quant Spectrosc RadiatTransf (JQSRT) 2021;272:107820. doi:10.1016/j.jqsrt.2021.107820.

[2] Grundmann S, Serov V, Trinter F. Revealing the two-electron cusp in the ground states of He and H_2 via quasifree double photoionization. Phys Rev Res 2020;2:033080. doi:10.1103/PhysRevResearch.2.033080.

[3] Weigold E, McCarthy IE. Electron momentum spectroscopy. NY: Kluwer; 1999.

[4] Neudatchin VG, Popov YV, Smirnov Y. Electron momentum spectroscopy of atoms, molecules and thin films. Physics– Uspekhi 1999;42:1017–44. doi:10.1070/PU1999v042n10ABEH000492.

[5] Popov YV, Dal Cappello C, K Kouzakov K. (e,3e) electronic momentum spectroscopy: advantages and perspectives. J Phys B At Mol Opt Phys 1996;29:5901–8. doi:10.1088/0953-4075/29/23/029.

[6] Watanabe N, Khajuria Y, Takahashi M, Udagawa Y, P S Vinitsky PS, Yu V P, Chuluunbaatar O, K A Kouzakov KA. (e,2e) and (e,3-1e) studies on double processes of he at large momentum transfer. Phys Rev A 2005;72:032705. doi:10.1103/PhysRevA.72.032705.

[7] Bothe W, Geiger H. Über das Wesen des Comptoneffekts; ein experimenteller Beitrag zur Theorie der Strahlung. Z Physik 1925;32:639–63.

[8] Bohr N, Kramers HA, Slater JC. The quantum theory of radiation. Phil Mag 1924;47:785–802. doi:10.1080/14786442408565262.

[9] Ullrich J, et al. Recoil-ion and electron momentum spectroscopy: reaction-microscopes. Rep Prog Phys 2003;66:1463–545. doi:10.1088/0034-4885/66/9/203.

[10] Kircher M, et al. Kinematically complete experimental study of Compton scattering at helium atoms near the threshold. Nat Phys 2020;16:756–60. doi:10.1038/s41567-020-0880-2.

[11] Spielberger L, Jagutzki O, Dörner R. Separation of photoabsorption and Compton scattering contributions to he single and double ionization. Phys Rev Lett 1995;74:4615. doi:10.1103/PhysRevLett.74.4615.

[12] Spielberger L, Jagutzki O, Krässig B. Double and single ionization of helium by 58-kev x rays. Phys Rev Lett 1996;76:4685. doi:10.1103/PhysRevLett.76.4685.

[13] Krässig B, Dunford RW, Gemmell DS. Compton double ionization of helium in the region of the cross-section maximum. Phys Rev Lett 1999;83:53. doi:10.1103/PhysRevLett.83.53.

[14] Kircher M., Trinter F., Grundmann S. et al. Ion and electron momentum distributions from single and double ionization of helium induced by Compton scattering. ArXiv: 2110.09831v1 [physics.atom-ph], 19.10.2021.

[15] Bergstrom Jr PM, Surić PKT, Pratt RH. Compton scattering of photons from bound electrons: full relativistic independent-particle-approximation calculations. Phys Rev A 1993;48:1134–62. doi:10.1103/PhysRevA.48.1134.

[16] Kramers HA, Heisenberg W. Über die Streuung von Strahlung durch Atome. Z Physik 1925;31:681–708.

[17] Waller I, Hartree DR. On the intensity of total scattering of x-rays. Proc Roy Soc 1929;124:119–42. A

[18] Houamer S, Chuluunbaatar O, Volobuev IP, Popov YV. Compton ionization of hydrogen atom near threshold by photons in the energy range of a few kev: nonrelativistic approach. Eur Phys J D 2020;74:81–9. doi:10.1140/epjd/e2020-100572-1.

[19] Hahn T. Cuba – a library for multidimensional numerical integration. Comput Phys Commun 2005;168:78–95. https://www.sciencedirect.com/science/article/pii/S0010465505000792?via%3Dihub

[20] J. Berntsen J., T. O. Espelid T.O., Genz A.. Algorithm 698: DCUHRE: an adaptive multidemensional integration routine for a vector of integrals. 1991. ACM Trans Math Softw(The routine is given in http://www.math.wsu.edu/faculty/genz/software/fort77/dcuhre.f). 17, 4, 452–456, 10.1145/210232.210234.

[21] http://www.feynarts.de/cuba/ (The routine from CUBA library).
[22] Lewis Jr RR. Potential scattering of high-energy electrons in second born approximation. Phys Rev 1956;10:537–43. doi:10.1103/PhysRev.102.537.
[23] Chuluunbaatar O, Puzynin IV, Vinitsky PS, Popov YV, Kouzakov KA, Cappello CD. Role of the cusp conditions in electron-helium double ionization. Phys Rev A 2006;74:014703. doi:10.1103/PhysRevA.74.014703.
[24] Brauner M, Briggs JS, Klar H. Triply-differential cross sections for ionisation of hydrogen atoms by electrons and positrons. J Phys B 1989;22:2265–88. doi:10.1088/0953-4075/22/14/010.
[25] Richter RH, et al. Design and technology of DEPFET pixel sensors for linear collider applications. Nucl Instrum Methods Phys Res A 2003;511:250–6. doi:10.1016/S0168-9002(03)01802-3.